Molecular Shuttles Based on Tetrathiafulvalene Units and 1,5-Dioxynaphthalene Ring Systems

Seogshin Kang, Scott A. Vignon, Hsian-Rong Tseng, and J. Fraser Stoddart*[a]

Abstract: Six different degenerate [2]rotaxanes were synthesized and characterized. The rotaxanes contained either two tetrathiafulvalene (TTF) units or two 1,5-dioxynaphthalene (DNP) ring systems, both of which serve as recognition sites for a cyclobis(paraquat-*p*-phenylene) ($CBPQT^{4+}$) ring. Three different spacer units were incorporated into the dumbbell components of the [2]rotaxanes between the recognition sites. They include a polyether chain, a terphenyl unit, and a diphenyl ether linker, all of which were investigated in order to probe the effect of the spacers on the rate of the shuttling process. Data from dynamic ^{1}H NMR spectroscopy revealed a relatively small difference in the $\Delta G^{\neq}$ values for the shuttling process in the [2]rotaxanes containing the three different spacers, in contrast to a large difference between the TTF-containing rotaxanes (18 kcal mol^{-1}) and the DNP-containing rotaxanes (15 kcal mol^{-1}). This 3 kcal mol^{-1} difference is predominantly a result of a ground-state effect, reflecting the much stronger binding of TTF units to the $CBPQT^{4+}$ ring in comparison with DNP ring systems. An examination of the enthalpic ($\Delta H^{\neq}$) and entropic ($\Delta S^{\neq}$) components for the shuttling process in the DNP-containing rotaxanes revealed significant differences between the three spacers, a property which could be important in designing new molecules for incorporation into molecular electronic and nanoelectromechanical (NEMs) devices.

Keywords: molecular shuttles · nanotechnology · NMR spectroscopy · rotaxanes · self-assembly · template synthesis

Introduction

In recent years, the convergence of two areas of scientific endeavor, namely the design and synthesis of mechanically interlocked compounds[1,2] and solid-state molecular electronic devices,[3] has led to many significant and unexpected discoveries. The incorporation of these compounds, that is, catenanes and rotaxanes containing mechanical bonds, into solid-state devices has led to the demonstration[4] of high-density molecular memory and logic devices. Despite some skepticism, a number of such devices incorporating different electrodes[5] and molecular switches[6] have been demonstrated to operate by mechanisms that are believed to be similar to those observed in solution[7,8] and in half-devices.[9] In spite of these numerous examples, a number of questions still remain to be answered with regard to the detailed mechanism of operation of full, two-terminal devices. One of the main questions surrounding the full devices relates to the precise mechanism operating within the single monolayer of mechanically-interlocked bistable catenanes[7] or rotaxanes[8] sandwiched between the two electrodes.

The collaboration between our group at UCLA and the Heath group at Caltech has resulted[4a–d] in the incorporation of numerous bistable [2]catenanes and [2]rotaxanes into molecular-switch tunnel junctions (MSTJs). Such devices are constructed by depositing a Langmuir–Blodgett (LB) monolayer[10] of molecules onto a patterned bottom electrode, which has been either polysilicon[4a–c] or a semiconducting carbon nanotube,[4d] but never a metal. This step is then followed by the electron beam (e-beam) deposition of a top electrode, composed of a layer of Ti followed by a layer of Al. A schematic of such a device, composed of a polysilicon bottom electrode and a monolayer of amphiphilic bistable [2]rotaxanes, and its proposed mode of operation is shown in Figure 1. The fabricated device can be switched between high and low conductivity states by applying ± 2 V. If the higher conducting, or metastable ("ON") state of the switch is left unperturbed, it will undergo a thermal relaxation back to the lower conducting, ground ("OFF") state of the switch. Also, in keeping with a thermally activated process, it has been observed that, if the device is cooled down to

[a] S. Kang, S. A. Vignon, Dr. H.-R. Tseng, Prof. J. F. Stoddart
California Nanosystems Institute and
Department of Chemistry and Biochemistry
University of California, Los Angeles
405 Hilgard Avenue, Los Angeles, CA 90095–1569 (USA)
Fax: (+1) 310-206-1843
E-mail: stoddart@chem.ucla.edu

 DOI: 10.1002/chem.200305725

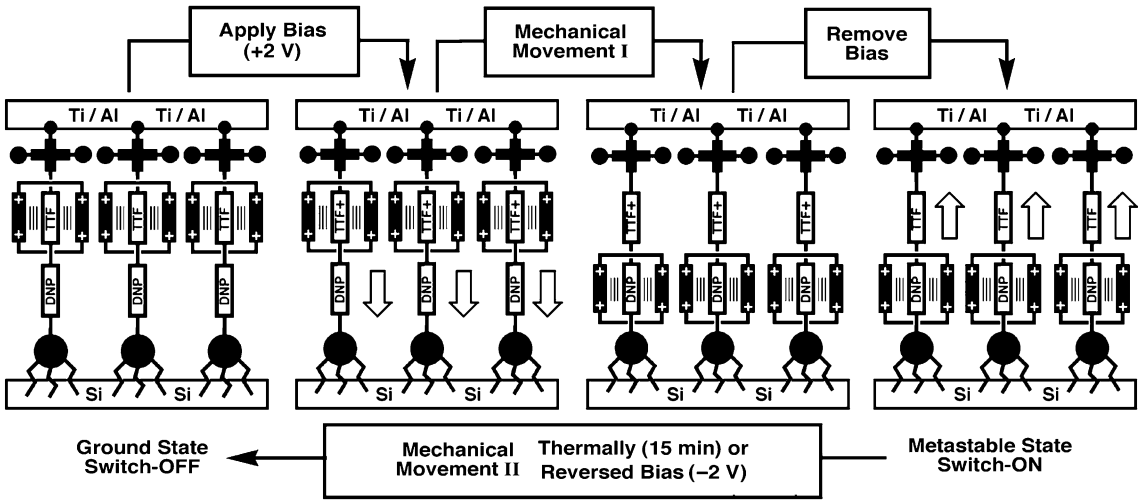

Figure 1. Schematic idealized representation of a molecular switch tunnel junction (MSTJ) composed of a bottom polysilicon electrode, a monolayer of amphiphilic bistable [2]rotaxanes, and a top electrode composed of Ti and Al. The proposed operating mechanism of the device is also shown. Application of +2 V oxidizes the TTF unit and causes movement of the $CBPQT^{4+}$ ring to the DNP ring system. After the voltage is removed, the TTF unit returns to its neutral form, but the ring remains on the DNP ring system in a metastable state. This state is a higher conducting one relative to the ground state, which is reached when the ring returns to the TTF unit through thermal relaxation or application of −2 V.

sufficiently low temperatures (~200 K), it can no longer be switched between these two states.[4a] These observations, together with results from many control experiments, suggest that an activated process, most likely an electromechanical one, is responsible for the switching "ON" and "OFF" of the device.[11]

The experimental results were certainly not unexpected, since these mechanically interlocked, switchable molecules had been designed specifically to undergo electrochemical switching. The bistable [2]catenanes[7] and [2]rotaxanes[8] are composed of two components, a tetracationic cyclophane, cyclobis(paraquat-*p*-phenylene) ($CBPQT^{4+}$), and either a two-station crown ether macrocycle in the case of the bistable [2]catenanes,[7] or a two-station dumbbell component in the case of the bistable [2]rotaxanes.[8] Within the crown ether and dumbbell components, the two stations must serve as very different recognition sites for the $CBPQT^{4+}$ ring. Examples of such recognition sites are a tetrathiafulvalene (TTF) unit and a 1,5-dioxynaphthalene (DNP) ring system. Being the much stronger π-electron donor, the TTF unit resides inside the $CBPQT^{4+}$ ring with greater than 99:1 preference over the DNP ring system (Figure 2a). However, if the TTF unit is oxidized to its mono- or dicationic form, then the molecules undergo a circumrotation or translational process so as to position the DNP ring system inside the $CBPQT^{4+}$ ring (Figure 2b). This mechanical movement can then be reversed by reducing the oxidized TTF unit (TTF^{+} or TTF^{2+}) back to its neutral form (TTF). However, a barrier ($\Delta G^{\ddagger}_{DNP}$) exists to this returning motion (Figure 2c)—one which, in solution, is overcome rapidly so that an equilibrium is established whereby, once again, the lower energy translational isomer dominates. In more restricted environments, however, the time it takes for the higher energy translational isomer (the metastable state) to return to the lower energy translational isomer (the ground state) can be expected to increase and does.[12]

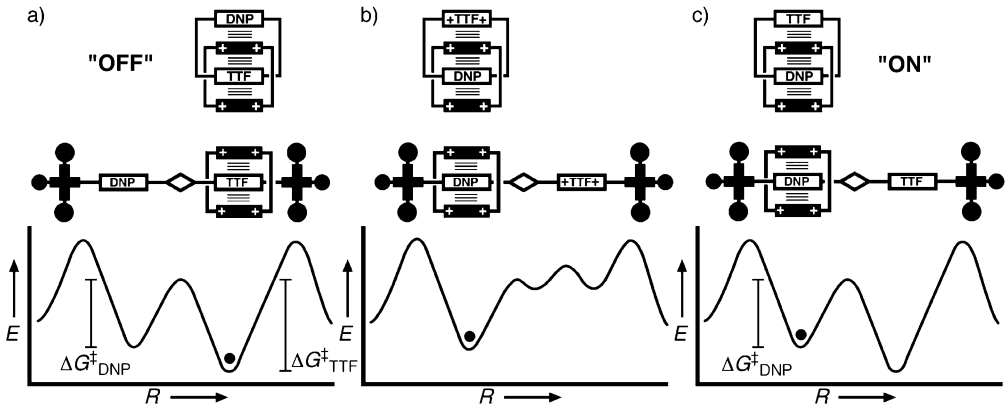

Figure 2. Schematic descriptions of the potential-energy surfaces for bistable [2]catenanes and [2]rotaxanes, a) in the neutral ground state, in which the lower energy isomer with the TTF unit inside the $CBPQT^{4+}$ ring constitutes the highly preferred translational isomer; b) in the oxidized state, in which the DNP ring system now resides exclusively within the $CBPQT^{4+}$ ring; and c) in the metastable state, in which the DNP ring system still resides within the $CBPQT^{4+}$ as a result of the barrier, $\Delta G^{\ddagger}_{DNP}$, to its return to the much lower energy translational isomer where the TTF unit is located inside the $CBPQT^{4+}$ ring.

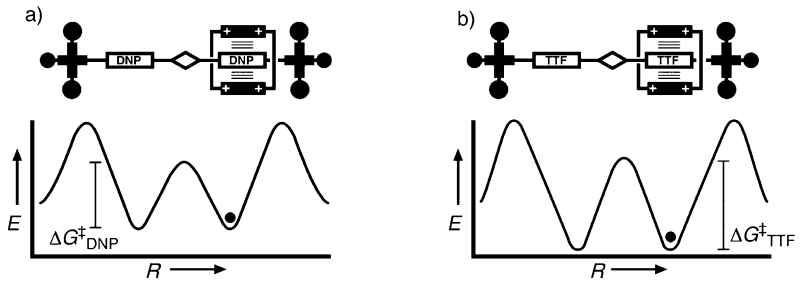

Figure 3. Schematic descriptions of the potential-energy surfaces for degenerate [2]rotaxanes that contain two identical recognition sites for the $CBPQT^{4+}$ ring, either a) both DNP ring systems or b) both TTF units.

Although this (electro)chemical switching mechanism has also been observed in solution employing both UV-visible[8c] and ^{1}H NMR[8c,13] spectroscopy, the kinetics associated with the switching process cannot be measured by using these techniques, because it occurs too rapidly. It would be possible to determine $\Delta G^{\ddagger}_{TTF}$ and $\Delta G^{\ddagger}_{DNP}$ (Figure 2) for these nondegenerate, two-station catenanes[14] and rotaxanes[15] by studying the circumrotation or shuttling exchange processes, respectively, that occur within them, except that this possibility is precluded by the fact that far too little of the higher energy translational isomer with the DNP ring system inside the $CBPQT^{4+}$ ring is present to detect in these spectroscopic experiments. One way to avoid this problem is to design and synthesize model systems that are similar enough to the nondegenerate systems, such that the energy barriers for the circumrotation and shuttling processes will be very similar in the two systems. Here, we present one approach to this problem that involves synthesizing degenerate, two-station rotaxanes whereby both recognition sites positioned along the dumbbell component of the [2]rotaxane are identical, that is, either both TTF units or both DNP ring systems, so that the exchange process (shuttling[15]) between two isoenergetic forms (Figure 3) can be easily observed by dynamic ^{1}H NMR spectroscopy.

In addition to comparing the shuttling rates in molecular shuttles containing dual TTF and DNP stations, it was also possible for us to incorporate different spacer units into the degenerate [2]rotaxanes between the two recognition sites. Since the $CBPQT^{4+}$ ring must pass over these spacer units to move from one site to the other, by changing the size and/or functionality associated with these spacer units, it should be possible to influence the shuttling speed. Three different spacer units were incorporated into the range of molecular shuttles in order to determine their influence. Here we will describe 1) the template-directed synthesis[16] of the six degenerate [2]rotaxanes, **1**·4 PF_6–**6**·4 PF_6, shown in Figure 4, and their corresponding dumbbell components, **7**--**12**; 2) the complete characterization of all

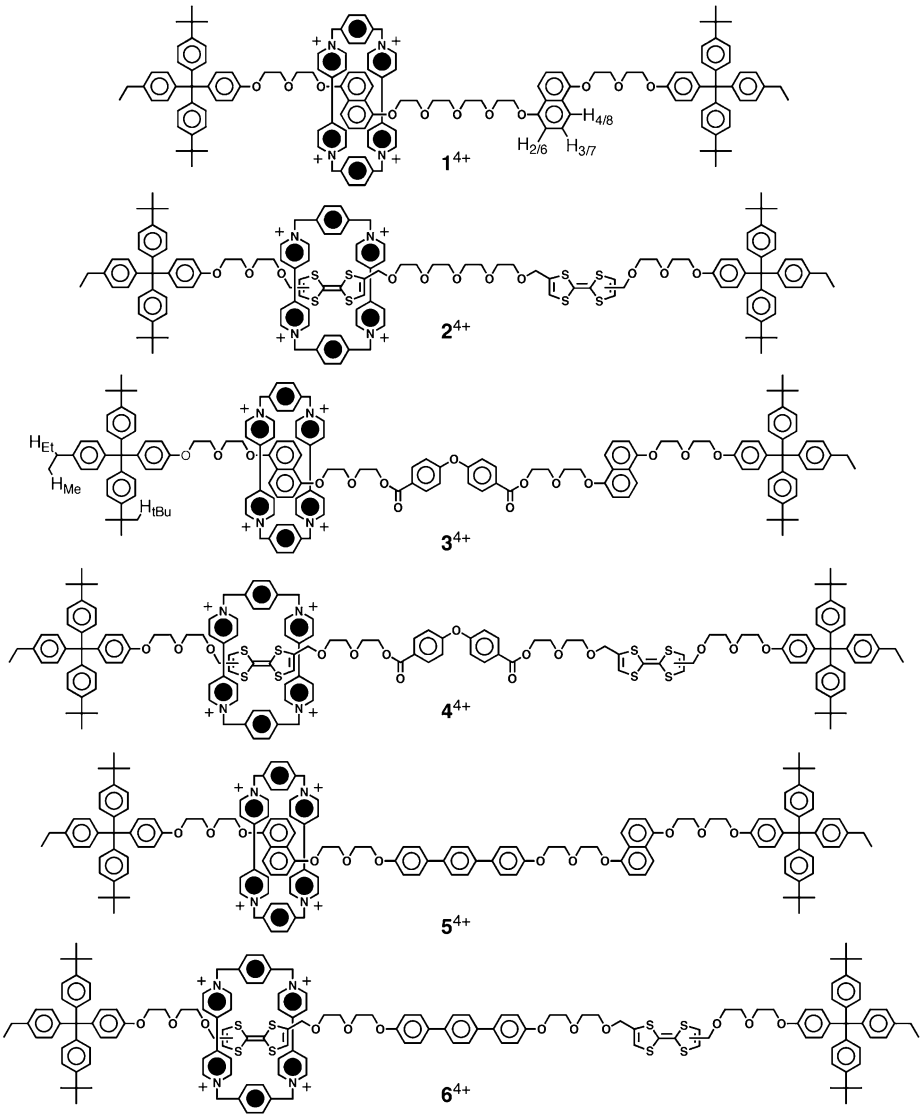

Figure 4. The structural formulas for the six degenerate [2]rotaxanes, **1**·4 PF_6–**6**·4 PF_6, containing either two TTF units or two DNP ring systems. Also shown are the labels for the protons used to study the shuttling process.

the molecular shuttles; and 3) a dynamic ^{1}H NMR spectroscopic study of the shuttling rates in all of these compounds.

Results and Discussion

Design and synthetic strategy: Retrosynthetic analyses of the degenerate [2]rotaxanes **1**·4PF$_6$–**6**·4PF$_6$, and their corresponding precursor dumbbell-shaped compounds **7–12** led to the following considerations and strategies. Common, of course, to all six syntheses is the final clipping reaction to form (Schemes 1 and 2) the CBPQT^{4+} ring around each of the six dumbbell-shaped compounds. It is a template-directed procedure.[16] The conventional syntheses (Schemes 1 and 2) of the DNP-containing dumbbell-shaped compounds **7**, **9**, and **11** rely upon two key starting materials, namely, the alcohol **3** and its tosylate[17] **14**, which are co-joined directly by nucleophilic substitution to give **7** or to one or two spacers, namely **19** and **20** by esterification and nucleophilic substitution, respectively, to afford **9** and **11**. Under essentially similar conditions, the syntheses of the three TTF-containing dumbbell-shaped compounds **8**, **10**, and **12** have been achieved (Schemes 1 and 2) starting from precursors which include the alcohol **15** and its tosylate **16**, as well as the two spacers **19** and **20** where appropriate.

Synthesis: The routes employed in the syntheses of the degenerate, two-station [2]rotaxanes **1**·4PF$_6$ and **2**·4PF$_6$, and their corresponding dumbbell-shaped compounds **7** and **8**, respectively, are outlined in Scheme 1. The dumbbell-shaped compound **7** was obtained in 87% yield by alkylating the alcohol[18] **13** with the tosylate **14** in the presence of NaH as base. The dumbbell-shaped compound **7** was then used as the template in a template-directed synthesis[16] of the [2]rotaxane **1**·4PF$_6$. A CBPQT^{4+} ring was clipped onto the dumbbell-shaped template from its dicationic precursor[19] **18**·2PF$_6$ and α,α′-dibromoxylene (**17**) to give the [2]rotaxane **1**·4PF$_6$ in 54% yield, as an analytical pure, purple solid after chromatography on silica gel using a 1% NH_4PF_6 solution in Me_2CO as eluent. Similarly, the TTF-containing [2]rotaxane **2**·4PF$_6$ and its dumbbell-shaped precursor **8** were prepared from the alcohol[8c,13] **15** with the tosylate[8c,13] **16**, in 82% and 51%, respectively, by using the reaction and isolation conditions similar to those employed in the preparations of **7** and **1**·4PF$_6$.

The preparation of the dumbbell-shaped compounds **9–12** and their corresponding [2]rotaxanes **3**·4PF$_6$–**6**·4PF$_6$, are summarized in Scheme 2. In pathway I, the dumbbell-shaped compounds **9** and **10** were obtained in 95% and 97% yields by a diesterfication of 4,4′-oxybis(benzoic acid) (**19**) with two equivalent of the alcohols **13** and **15**, respectively. In pathway II, dialkylation of 4,4″-dihydroxy-*p*-terphenyl[20] (**20**) with the tosylates **14** and **16**, in the presence of K_2CO_3, LiBr, and [18]crown-6 in DMF, gave the dumbbell-shaped compounds **11** and **12** in 90% and 63% yields, respectively. Once again, the [2]rotaxanes **3**·4PF$_6$–**6**·4PF$_6$ were obtained in 25%, 11%, 25%, and 51% yields, respectively, by applying a template-directed protocol[16] in which

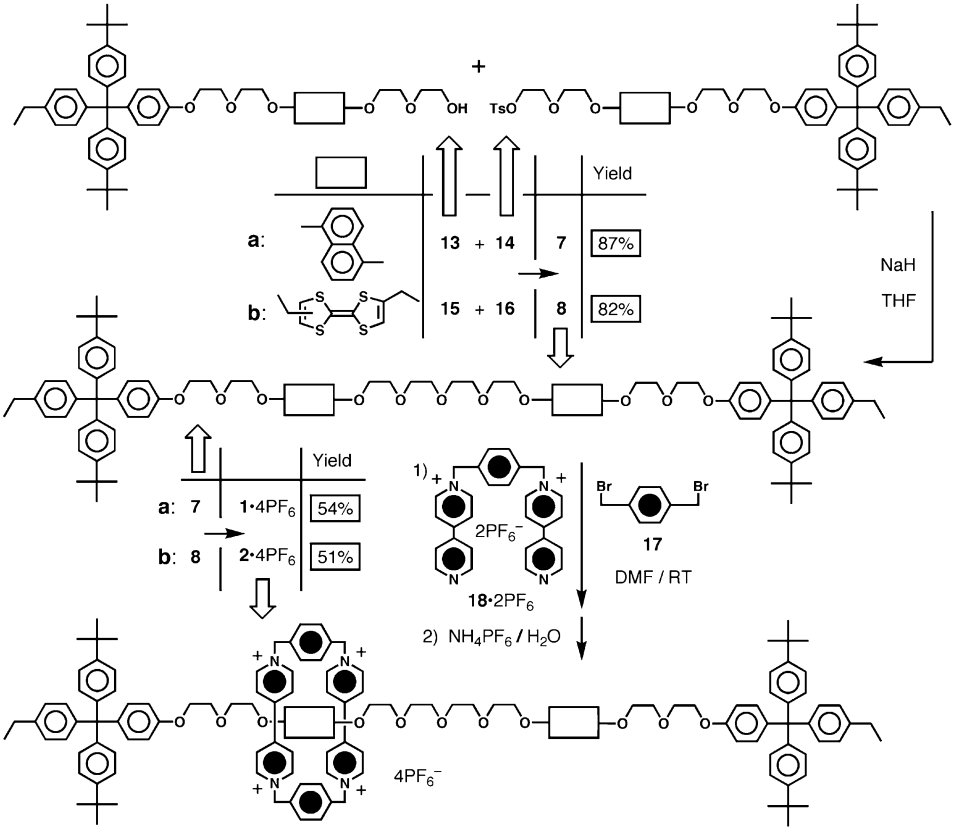

Scheme 1. The syntheses of the [2]rotaxanes **1**·4PF$_6$ and **2**·4PF$_6$.

the dumbbell-shaped compounds were treated with the dicationic precursor **18**·2 PF_6 and α,α′-dibromoxylene (**17**) in DMF at room temperature.

Dynamic ^{1}H NMR spectroscopy: The shuttling processes in the six degenerate [2]rotaxanes, namely **1**·4 PF_6–**6**·4 PF_6, were investigated by acquiring ^{1}H NMR spectra of each rotaxane at a variety of different temperatures in CD_3COCD_3. In these rotaxanes, the $CBPQT^{4+}$ ring is located on one of two identical stations and shuttles back and forth between these two degenerate forms. At lower temperatures, this shuttling process becomes slow on the ^{1}H NMR timescale and the signals in the ^{1}H NMR spectrum separate into pairs of equal intensity signals. This separation is most evident when observing the ^{1}H NMR signals (Figure 5) for the alkyl protons on the hydrophobic stoppers. The chemical shifts for these protons in the dioxynaphthalene-containing rotaxanes **1**·4 PF_6, **3**·4 PF_6 and **5**·4 PF_6 at high and low temperature are listed in Table 1. Quantitative analysis of this shuttling process was accomplished by using two methods. Spin saturation transfer[21] (SST) was used to determine the rate of shuttling in the slow-exchange regime and line-shape analysis[22] (LSA) (see Figure 6 for example spectra) was used over the entire range. The data are summarized in Tables 2–4. From this data, it is apparent that the $\Delta G^{\ddagger}$ values for shuttling in all of these three rotaxanes are all within ~ 0.5 kcal mol^{-1} of each other. Thus, very little difference is observed between the shuttling processes in rotaxanes con-

Table 1. ^{1}H NMR chemical shift values for select protons of the degenerate 1,5-dioxynaphthalene-containing rotaxanes **1**·4 PF_6, **3**·4 PF_6, and **5**·4 PF_6 at high and low temperature in CD_3COCD_3 at 500 MHz.

	Assignment[a]	Limiting δ values[b]	T [K]	Limiting δ values[c]	T [K]
1·4 PF_6	H_{tBu}	1.20, 1.27	236	1.30	326
	H_{Et}	2.52, 2.58	236	2.61	315
	H_{Me}	1.11, 1.17	236	1.21	326
3·4 PF_6	H_{tBu}	1.25, 1.28	232	1.32	327
	H_{Et}	2.56, 2.59	232	2.63	317
	H_{Me}	1.15, 1.19	232	1.23	327
5·4 PF_6	H_{tBu}	1.22, 1.25	236	1.29	316
	H_{Et}	2.54, 2.57	236	2.60	316
	H_{Me}	1.12, 1.15	236	1.20	316

[a] Assignments for these protons are given in Figure 4. [b] Low temperature. [c] High temperature.

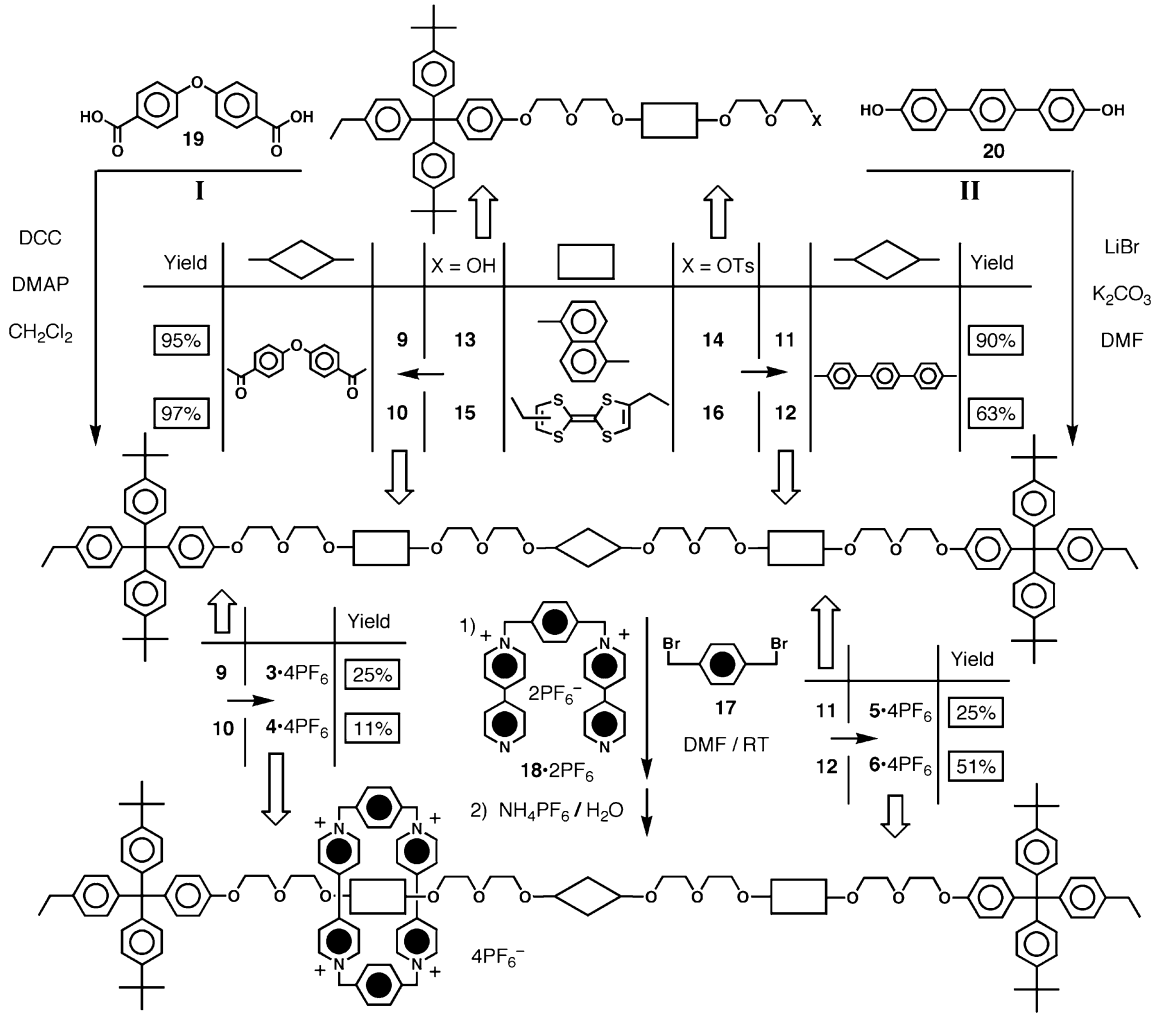

Scheme 2. The syntheses of the [2]rotaxanes **3**·4 PF_6–**6**·4 PF_6.

Table 2. Kinetic and thermodynamic data for shuttling in the [2]rotaxane **1**·4PF_6 in CD_3COCD_3.

T [K][a]	k_{ex} [s^{-1}]	$\Delta G^{\neq}$ [kcal mol^{-1}][b]
247	0.2[c]	15.2
255	0.7[c]	15.3
259	0.8[d]	15.2
271	3[d]	15.2
282	8[d]	15.3
293	20[d]	15.4
305	47[d]	15.5

[a] Calibrated using neat MeOH sample. [b] ± 0.1 kcal mol^{-1}. [c] These data were obtained by the spin saturation transfer[21] (SST) method. Exchange was observed between the resonances for H_{Me} (Figure 4) at $\delta =$ 1.15/1.20 ppm. [d] These data were obtained by the line shape analysis[22] (LSA) method. The signals corresponding to H_{Et} (Figure 4) at $\delta = 2.52/2.58$ ppm were simulated.

Table 3. Kinetic and thermodynamic data for shuttling in the [2]rotaxane **3**·4PF_6 in CD_3COCD_3.

T [K][a]	k_{ex} [s^{-1}]	$\Delta G^{\neq}$ [kcal mol^{-1}][b]
248	0.2[c]	15.3
259	0.7[c]	15.3
270	1.8[c]	15.4
282	4.7[c]	15.6
270	2[d]	15.4
282	6[d]	15.5
294	19[d]	15.5
304	55[d]	15.4
317	120[d]	15.6

[a] Calibrated using neat MeOH sample. [b] ± 0.1 kcal mol^{-1}. [c] These data were obtained by the spin saturation transfer[21] (SST) method. Exchange was observed between the resonances for Ht_{Bu} (Figure 4) at $\delta =$ 1.27/1.30 ppm. [d] These data were obtained by the line shape analysis[22] (LSA) method. The signals corresponding to H_{Et} (Figure 4) at $\delta = 2.56/2.59$ ppm were simulated.

Table 4. Kinetic and thermodynamic data for shuttling in the [2]rotaxane **5**·4PF_6 in CD_3COCD_3.

T [K] [a]	k_{ex} [s^{-1}]	$\Delta G^{\neq}$ [kcal mol^{-1}][b]
236	0.1[c]	14.8
247	0.4[c]	14.9
259	1.5[c]	14.9
247	0.4[d]	14.8
258	1.4[d]	14.9
270	4.4[d]	15.0
282	13[d]	15.0
293	33[d]	15.1
305	85[d]	15.2

[a] Calibrated using neat MeOH sample. [b] ± 0.1 kcal mol^{-1}. [c] These data were obtained by the spin saturation transfer[21] (SST) method. Exchange was observed between the resonances for $H_{2/6}$ (Figure 4) at $\delta =$ 2.26/7.33 ppm. [d] These data were obtained by the line shape analysis[22] (LSA) method. The signals corresponding to H_{Et} (Figure 4) at $\delta = 2.54/2.57$ ppm were simulated.

taining the three different spacers considering $\Delta G^{\neq}$ values alone.

Quantitative analyses of the shuttling processes in rotaxanes **2**·4PF_6, **4**·4PF_6 and **6**·4PF_6 were precluded by the presence of multiple isomers arising from the different possible

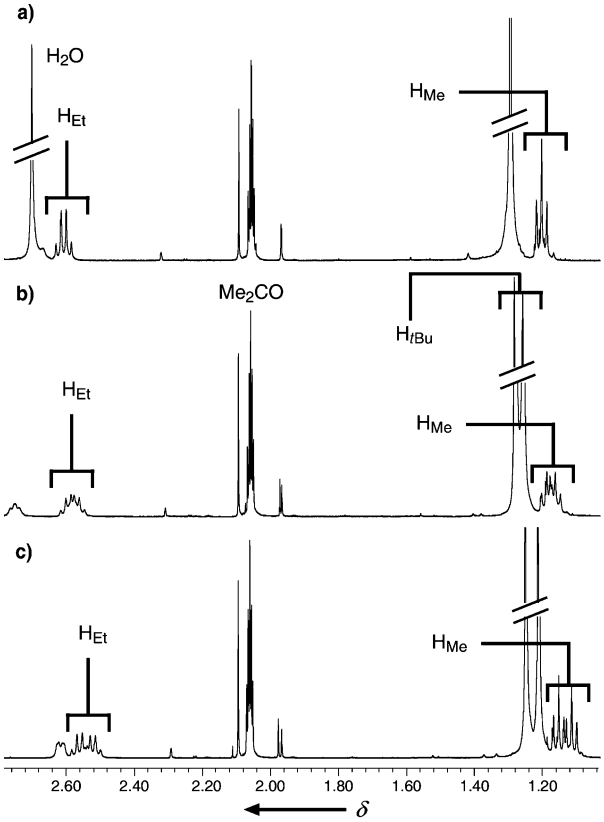

Figure 5. Partial ^{1}H NMR spectra for **5**·4PF_6 in CD_3COCD_3 recorded at a) 316 K, b) 282 K, and c) 226 K. The resonances corresponding to the protons on the hydrophobic stopper are labeled. Structural assignments for these protons can be found in Figure 4. Note that at lower temperatures, the signals for Me, Et (CH_2CH_3) and *t*Bu separate out into two triplets, two quartets, and two singlets, respectively: at higher temperatures one triplet, one quartet, and one singlet are observed as a result of coalescence of the respective signals.

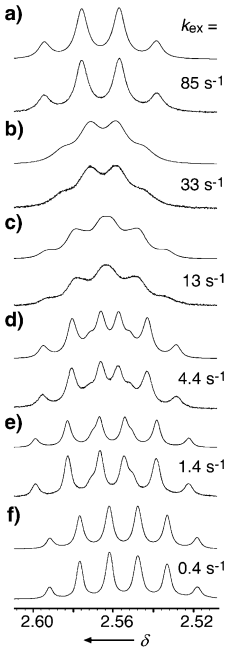

Figure 6. The simulated (top) and experimental (bottom) partial ^{1}H NMR spectra for the resonances of the H_{Et} protons (Figure 4) of **5**·4PF_6 at a) 305 K, b) 293 K, c) 282 K, d) 270 K, e) 258 K, and f) 247 K.

substitution patterns on the TTF moiety (referred to here as *cis* and *trans*). Thus, there are four possible exchange processes that can occur, with the $CBPQT^{4+}$ ring moving from *cis*-to-*trans*, *trans*-to-*cis*, *cis*-to-*cis*, or *trans*-to-*trans*. Although it would be interesting to study the different rates of shuttling between these isomers and the relative preference of the ring for one isomer over the other, it was not possible to identify these isomers in the ^1H NMR spectrum well enough to analyze the shuttling process. It was, however, possible to estimate[23] that the $\Delta G^{\neq}$ value for shuttling between the two TTF sites is ~17–18 kcal mol^{-1} by observing the coalescences of the many peaks corresponding to the different isomers.

In order to investigate more deeply the different effects of the three spacers on the shuttling process, the $\Delta H^{\neq}$ and $\Delta S^{\neq}$ values were deduced from the graphs shown in Figure 7. An examination of this data (Table 5) reveals significant differences for the three different spacers. The glycol chain spacer has the largest entropic penalty (large negative $\Delta S^{\neq}$) associated with a reduction in the conformational flexibility in the transition state. On the other hand, the enthalpic penalty for shuttling over the glycol chain spacer is the smallest of the three, presumably because of favorable electrostatic interactions between the partially negative oxygen atoms and the $CBPQT^{4+}$ ring, and also the smaller size relative to the aromatic spacers. The terphenyl and diester spacers have similar entropic penalties and are smaller than that for the glycol spacer. This result is not suprising on account of the more rigid nature of these aromatic-ring-containing spacers. The largest enthalpic penalty of the three spacers is found to be for the diester-containing spacer, perhaps resulting from the "bent" nature of the spacer resulting from the bisphenyloxy linkage, compared to the linear terphenyl spacer. Enthalpic versus entropic considerations will be important when designing molecules to operate as molecular machines and switches in the solid state. The operating temperatures will also have to be considered when choosing the optimal spacer to incorporate into the molecular design. In order to construct devices where the shuttling or switching barrier does not change dramatically with temperature, more rigid aromatic spacers will need to be used.

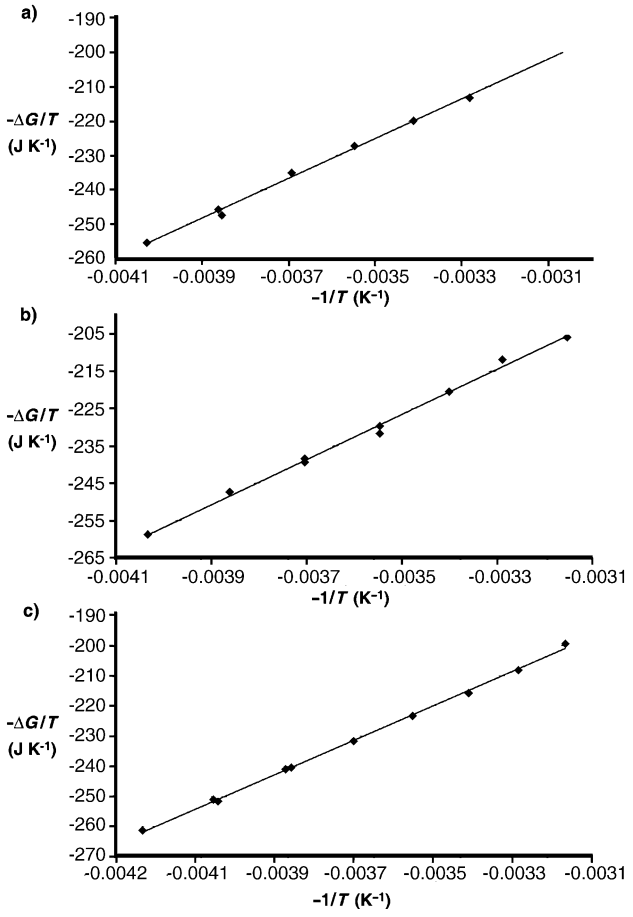

Figure 7. Eyring plots created from the data in Tables 2–4 for the degenerate rotaxanes a) **1**·4 PF_6, b) **3**·4 PF_6, and c) **5**·4 PF_6. The values for $\Delta H^{\neq}$ and $\Delta S^{\neq}$ were obtained from the slopes and intercepts of these plots, respectively, and are given in Table 5.

Table 5. Activation parameters for shuttling in the [2]rotaxanes **1**·4 PF_6, **3**·4 PF_6, and **5**·4 PF_6 in CD_3COCD_3.

	$\Delta H^{\neq}$ [kcal mol^{-1}]	$\Delta S^{\neq}$ [cal mol K^{-1}]
1·4 PF_6	12.7	−9.3
3·4 PF_6	14.5	−3.2
5·4 PF_6	13.6	−4.8

Conclusion

In this paper, kinetic and thermodynamic data have been presented for shuttling of a $CBPQT^{4+}$ ring component in a series of degenerate [2]rotaxanes containing either two TTF units or two DNP ring systems in their dumbbell components as recognition sites for the ring. These degenerate molecular shuttles serve as models to study the barriers to ring movement in the nondegenerate bistable [2]rotaxanes used in molecular electronic devices.[4] It has been found that the barrier for shuttling between two DNP ring systems is ~15 kcal mol^{-1}, while in the case of two TTF units the barrier increases to ~17–18 kcal mol^{-1}. The difference observed between these two molecular shuttles arises primarily from a ground-state effect, reflecting the difference in binding constants of the TTF unit ($K_a = 500\,000\ \mathrm{M}^{-1}$ in CD_3CN, $\Delta G^{\circ}_{298} = -8$ kcal mol^{-1})[24] versus the DNP ring system ($K_a = 25\,000\ \mathrm{M}^{-1}$ in CD_3CN, $\Delta G^{\circ}_{298} = -6$ kcal mol^{-1}),[25] each carrying two diethyleneglycol substituents, with a $CBPQT^{4+}$ ring. Additionally, the effect of the spacers on the $\Delta G^{\neq}$ values was shown to be minimal. When the enthalpic and entropic activation parameters, namely $\Delta H^{\neq}$ and $\Delta S^{\neq}$, were determined, large differences were observed. In an upcoming review article, this thermodynamic data will be compared to data for similar processes in more restricted environments, such as half-devices and full-devices, to provide further evidence that the mechanism operating across all of these regimes is a common one, namely a mechanical ring movement.

Experimental Section

General methods: Chemicals were purchased from Aldrich and used as received. The alcohols **13**[16] and **15**,[8c,13] the tosylate **16**,[8c,13] α,α′-[1,4-phenylenebis (methylene)]bis-(4,4′-bipyridium) bis(hexa-fluorophosphate) (**18**·2PF$_6$),[19] and 4,4′-dihydroxy-*p*-terphenylene (**20**)[20] were all prepared according to procedures reported in the literature. Solvents were dried following methods described in the literature. All reactions were carried out under an anhydrous argon atmosphere. Thin-layer chromatography (TLC) was performed on aluminum sheets coated with silica gel 60F (Merck 5554). The plates were inspected by UV light and, if required, developed in I_2 vapor. Column chromatography was carried out by using silica gel 60 (Merck 9385, 230–400 mesh). Melting points were determined on an Electrothermal 9100 melting point apparatus and are uncorrected. All ^{1}H and ^{13}C NMR spectra were recorded on either 1) a Bruker ARX400 (400 MHz and 100 MHz, respectively), 2) a Bruker ARX500 (500 MHz and 125 MHz, respectively), or 3) a Bruker Avance 500 (500 MHz and 125 MHz, respectively), using residual solvent as the internal standard. Samples were prepared by using $CDCl_3$, CD_3COCD_3, or CD_3CN purchased from Cambridge Isotope Laboratories. All chemical shifts are quoted using the δ scale, and all coupling constants (J) are expressed in Hertz (Hz). Electron impact ionization mass spectrometry (EIMS) was performed on a AUTO-SPEC instrument. Fast atom bombardment (FAB) mass spectra were obtained using a ZAB-SE mass spectrometer, equipped with a krypton primary atom beam, utilizing a *m*-nitrobenzyl alcohol matrix. Cesium iodide or poly(-ethylene glycol) were employed as reference compounds. Electrospray mass spectra (ESMS) were measured on a VG ProSpec triple focusing mass spectrometer with MeCN as the mobile phase. Microanalyses were performed by Quantitative Technologies, Inc.

Tosylate 14: A suspension of 4-[4-ethylphenyl-bis(4-*tert*-butylphenyl)methyl]phenol[26] (477 mg, 1.00 mmol), the ditosylate[27] of 1,5-bis[2(hydroxyethoxy)ethoxy]naphthalene (1.09 g, 1.69 mmol), K_2CO_3 (276 mg, 2.00 mmol), LiBr (10 mg, cat. amount), and [18]crown-6 (10 mg, cat. amount) in anhydrous MeCN (150 mL) was heated under reflux for two days. After cooling to room temperature, the mixture was filtered and the solid was washed with CH_2Cl_2. The combined organic phase was dried in vacuo and the residue was purified by column chromatography (SiO_2, EtOAc/hexane 1:3) to give the tosylate **14** (763 mg, 80%) as a colorless oil. ^{1}H NMR ($CDCl_3$, 500 MHz): δ=1.23 (t, J=7.6 Hz, 3H), 1.30 (s, 18H), 2.35 (s, 3H), 2.62 (q, J=7.6 Hz, 2H), 3.82 (t, J=4.7 Hz, 2H), 3.91 (t, J=4.7 Hz, 2H), 3.99 (t, J=4.8 Hz, 2H), 4.07 (t, J=4.8 Hz, 2H), 4.16 (t, J=4.9 Hz, 2H), 4.19 (t, J=4.7 Hz, 2H), 4.22 (t, J=4.7 Hz, 2H), 4.32 (t, J=4.9 Hz, 2H), 6.79 (d, J=7.5 Hz, 1H), 6.80–6.82 (m, 2H), 6.86 (d, J=7.5 Hz, 1H), 7.04–7.10 (m, 10H), 7.21–7.24 (m, 6H), 7.31 (dd, J=8.5, 7.5 Hz, 1H), 7.34 (dd, J=8.5, 7.5 Hz, 1H), 7.76–7.79 (m, 2H), 7.80 (d, J=8.5 Hz, 1H), 7.88 ppm (d, J=8.5 Hz, 1H); ^{13}C NMR ($CDCl_3$, 125 MHz): δ=15.3, 21.5, 28.2, 31.3, 34.2, 60.3, 63.1, 67.3, 67.8, 67.9, 68.9, 69.3, 69.8, 70.0, 105.6, 105.7, 113.1, 114.5, 114.7, 124.0, 125.0, 125.1, 126.5, 126.6, 126.7, 127.8, 129.7, 130.6, 131.0, 132.1, 132.9, 139.7, 141.3, 144.1, 144.5, 144.7, 148.2, 154.1, 154.3, 156.5 ppm; MS(FAB): *m/z* (%): 948 (20) $[M]^+$; elemental analysis calcd(%) for $C_{60}H_{68}O_8S$: C 75.92, H 7.22; found: C 75.93, H 7.28.

General procedure for the preparation of the dumbbell-shaped compounds 7 and 8: A mixture of the alcohols **13**[16] or **15**[8c,13] (0.600 mmol) and NaH (4.8 mmol) in dry THF (20 mL) was heated under reflux for 30 min, and a solution of the tosylate **14** or **16**[8c,13] (639 mg, 0.673 mmol), respectively, in THF (5 mL) was then added into the mixture. The reaction mixture was heated and stirred under reflux for 16 h. After cooling down to room temperature, H_2O was added to the mixture. The mixture was then extracted with CH_2Cl_2 (3×50 mL) and brine, and dried ($MgSO_4$). The solvent was removed and the residue was subjected to column chromatography (SiO_2, EtOAc/Hexane: 1/2) to give the dumbbell-shaped compounds.

Compound 7: Yield: 87%; ^{1}H NMR (CD_3COCD_3, 500 MHz): δ=1.16 (t, J=7.5 Hz, 6H), 1.25 (s, 36H), 2.57 (q, J=7.5 Hz, 4H), 3.61 (t, J=4.5 Hz, 4H), 3.67 (t, J=4.4 Hz, 4H), 3.86–3.91 (m, 8H), 3.93–3.97 (m, 4H), 4.06–4.11 (m, 4H), 4.16–4.20 (m, 4H), 4.20–4.24 (m, 4H), 6.75–6.80 (m, 4H), 6.83 (d, J=6.2 Hz, 2H), 6.85 (d, J=6.2 Hz, 2H), 7.03–7.09 (m, 20H), 7.23–7.29 (m, 12H), 7.80 (d, J=8.4 Hz, 2H), 7.81 ppm (d, J=8.4 Hz, 2H); ^{13}C NMR (CD_3COCD_3, 125 MHz): δ=14.8, 19.8, 27.8, 30.7, 33.8, 63.0, 67.3, 67.8, 69.3, 69.4, 69.6, 70.4, 70.6, 105.5, 105.6, 113.1, 114.1, 114.2, 124.0, 124.0, 125.0, 125.0, 126.6, 130.4, 130.7, 131.8, 139.3, 141.3, 144.3, 144.6, 148.1, 154.3, 154.3, 156.8, 169.9 ppm; MS (FAB): *m/z* (%): 1572 (100) $[M+1]^+$; elemental analysis calcd(%) for $C_{106}H_{122}O_{11}$: C 80.98, H 7.82; found: C 80.78, H 7.86.

Compound 8: Yield: 82%; ^{1}H NMR (CD_3COCD_3, 500 MHz): δ=1.18 (t, J=7.6 Hz, 6H), 1.27 (s, 36H), 2.58 (q, J=7.6 Hz, 4H), 3.56–3.60 (m, 20H), 3.64–3.66 (m, 4H), 3.77–3.79 (m, 4H), 4.08–4.10 (m, 4H), 4.28–4.29 (m, 8H), 6.47–6.50 (m, 4H), 6.80–6.82 (m, 4H), 7.05–7.10 (m, 20H), 7.27–7.29 ppm (m, 8H); ^{13}C NMR (CD_3COCD_3, 125 MHz): δ=14.9, 27.8, 29.1, 30.7, 33.8, 63.0, 67.2, 67.5, 67.5, 67.6, 69.1, 69.1, 69.1, 69.4, 69.4, 70.2, 70.3, 70.3, 70.3, 109.7, 113.1, 116.4, 116.5, 116.5, 124.1, 126.7, 130.4, 130.7, 131.8, 134.7, 134.7, 134.8, 134.8, 139.3, 141.3, 144.3, 144.6, 148.1, 156.8 ppm; MS(FAB): *m/z* (%): 1780 (100) $[M+1]^+$; elemental analysis calcd(%) for $C_{102}H_{122}O_{11}S_8$: C 68.80, H 6.91; found: C 68.72, H 6.86.

General procedure for the preparation of the dumbbell-shaped compounds 9 and 10: A suspension of the alcohols **13**[16] or **15**[8c,13] (0.33 mmol), 4,4′-oxybis(benzoic acid) (**19**) (39 mg, 0.15 mmol), DCC (129 mg, 0.60 mmol), and DMAP (73 mg, 0.60 mmol) in a solvent mixture containing CH_2Cl_2 (7 mL) and THF (20 mL) was stirred at room temperature for 24 h. After removal of solvent, the residue was purified by column chromatography (SiO_2, EtOAc/hexane 1:2) to give the dumbbell-shaped compounds.

Compound 9: Yield: 95%; ^{1}H NMR ($CDCl_3$, 500 MHz): δ=1.22 (t, J=7.6 Hz, 6H), 1.29 (s, 36H), 2.61 (q, J=7.6 Hz, 4H), 3.96–3.99 (m, 8H), 4.03 (t, J=4.9 Hz, 4H), 4.04 (t, J=4.9 Hz, 4H), 4.14 (t, J=4.7 Hz, 4H), 4.29 (t, J=4.9 Hz, 4H), 4.30 (t, J=4.9 Hz, 4H), 4.52 (t, J=4.7 Hz, 4H), 6.77–6.79 (m, 4H), 6.80 (d, J=7.7 Hz, 2H), 6.81 (d, J=7.7 Hz, 2H), 6.98 (d, J=8.8 Hz, 4H), 7.03–7.09 (m, 20H), 7.20–7.23 (m, 8H), 7.28 (dd, J=8.5, 7.7 Hz, 2H), 7.29 (d, J=8.5, 7.7 Hz, 2H), 7.84 (d, J=8.5 Hz, 2H), 7.85 (d, J=8.5 Hz, 2H), 8.04 ppm (d, J=8.8 Hz, 4H); ^{13}C NMR ($CDCl_3$, 125 MHz): δ=15.2, 28.2, 31.3, 34.2, 63.1, 64.1, 67.2, 67.8, 67.9, 69.4, 69.7, 69.9, 70.0, 105.6, 105.6, 113.1, 114.5, 114.7, 118.5, 124.0, 125.0, 125.0, 125.5, 126.6, 126.6, 126.7, 130.6, 131.0, 131.9, 132.1, 139.7, 141.3, 144.1, 144.5, 148.2, 154.2, 154.2, 156.7, 160.1, 165.8 ppm; MS(FAB): *m/z* (%): 1812 (88) $[M+1]^+$; elemental analysis calcd(%) for $C_{120}H_{130}O_{15}$: C 79.53, H 7.23; found: C, 79.07, H, 7.23.

Compound 10: Yield: 97%; ^{1}H NMR (CD_3COCD_3, 500 MHz): δ=1.19 (t, J=7.5 Hz, 6H), 1.30 (s, 36H), 2.61 (q, J=7.5 Hz, 4H), 3.60–3.64 (m, 8H), 3.66–3.71 (m, 8H), 3.80–3.84 (m, 8H), 4.09–4.10 (m, 4H), 4.29–4.31 (m, 8H), 4.43–4.45 (m, 4H), 6.43–6.47 (3×s, 4H), 6.81–6.83 (m, 4H), 7.09–7.16 (m, 20H), 7.30 (d, J=8.4 Hz, 8H), 8.09 ppm (d, J=8.5 Hz, 4H); ^{13}C NMR (CD_3COCD_3, 125 MHz): δ=14.9, 27.8, 29.3, 30.7, 33.8, 63.0, 63.8, 67.2, 67.6, 67.6, 68.8, 69.1, 69.4, 70.3, 70.3, 113.1, 116.3, 116.4, 116.5, 118.6, 124.0, 126.6, 130.4, 130.7, 131.7, 131.8, 139.3, 141.3, 144.3, 144.6, 148.1, 156.8, 160.1, 165.1, 204.3 ppm; MS (FAB): *m/z* (%): 2021 (97) $[M]^+$.

General procedure for the preparation of the dumbbell-shaped compounds 11 and 12: A solution of tosylates **14** or **16**[8c,13] (0.321 mmol), the terphenyl diol **20** (38 mg, 0.146 mmol), K_2CO_3 (61 mg, 0.437 mmol), LiBr (10 mg, cat. amount), and [18]crown-6 (10 mg, cat. amount) in anhydrous DMF (10 mL) was heated at 100 °C for 10 h. After cooling down to room temperature and removal of solvent, the mixture was extracted with CH_2Cl_2 (3×50 mL). The combined organic layers were dried ($MgSO_4$) and evaporated. The residue was purified by column chromatography (SiO_2, EtOAc/hexane/CH_2Cl_2 1:2:5) to give the dumbbell-shaped compound.

Compound 11: Yield: 90%; ^{1}H NMR ($CDCl_3$, 500 MHz): δ=1.25 (t, J=7.6 Hz, 6H), 1.31 (s, 36H), 2.64 (q, J=7.6 Hz, 4H), 3.99 (t, J=4.8 Hz, 4H), 4.04 (t, J=4.8 Hz, 4H), 4.07 (t, J=4.8 Hz, 4H), 4.10 (t, J=4.8 Hz, 4H), 4.16 (t, J=4.8 Hz, 4H), 4.24 (t, J=4.8 Hz, 4H), 4.31–4.35 (m, 8H), 6.81–6.83 (m, 4H), 6.85 (d, J=7.5 Hz, 2H), 6.86 (d, J=7.5 Hz, 2H), 7.03 (d, J=8.7 Hz, 4H), 7.06–7.12 (m, 20H), 7.23–7.26 (m, 8H), 7.33 (dd, J=8.4, 7.5 Hz, 2H), 7.34 (dd, J=8.4, 7.5 Hz, 2H), 7.56 (d, J=8.7 Hz, 4H), 7.61 (s, 4H), 7.89 (d, J=8.4 Hz, 2H), 7.90 ppm (d, J=8.4 Hz, 2H); ^{13}C NMR ($CDCl_3$, 125 MHz): δ=15.2, 28.1, 29.6, 31.3, 34.2, 63.1, 67.3, 67.6, 67.9, 67.9, 69.9, 70.0, 70.0, 105.7, 113.1, 114.6, 114.6, 114.9, 124.0, 125.0, 126.6, 126.7, 126.7, 126.9, 127.9, 130.6, 131.0, 132.1, 133.4, 139.0, 139.7, 141.3, 144.1, 144.5, 148.2, 154.2, 154.2, 156.5, 158.3 ppm; MS(FAB):

m/z (%): 1816 (100) $[M+1]^+$; elemental analysis calcd(%) for $C_{124}H_{134}O_{12}$: C 81.99, H 7.44; found: C 81.07, H 7.53.

Compound 12: Yield: 63%; ^{1}H NMR (CD_3COCD_3, 500 MHz): $\delta = 1.17$ (t, $J = 7.6$ Hz, 6H), 1.26 (s, 36H), 2.58 (q, $J = 7.6$ Hz, 4H), 3.56–3.64 (m, 12H), 3.64–3.68 (m, 4H), 3.75–3.80 (m, 4H), 3.81–3.83 (m, 4H), 4.06–4.09 (m, 4H), 4.15–4.18 (m, 4H), 4.28–4.30 (m, 8H), 6.46, 6.48, 6.49, 6.49 (4 × s, 4H), 6.79–6.82 (m, 4H), 7.01 (d, $J = 8.6$ Hz, 2H), 7.02 (d, $J = 8.6$ Hz, 2H), 7.05–7.11 (m, 20H), 7.26–7.28 (m, 8H), 7.59 (d, $J = 8.6$ Hz, 2H), 7.60 (d, $J = 8.6$ Hz, 2H), 7.63 ppm (s, 4H); ^{13}C NMR (CD_3COCD_3, 125 MHz): $\delta = 14.8$, 26.7, 27.8, 30.6, 33.8, 63.0, 67.2, 67.5, 67.6, 69.1, 69.2, 69.4, 69.4, 70.3, 70.4, 113.1, 114.9, 116.3, 116.4, 116.4, 116.5, 124.0, 126.6, 126.6, 127.6, 130.4, 130.7, 131.8, 134.7, 134.7, 134.8, 139.2, 139.2, 141.3, 144.3, 144.6, 148.1, 156.8, 158.6 ppm; MS(FAB): *m/z* (%): 2024 (100) $[M+1]^+$; elemental analysis calcd (%) for $C_{120}H_{134}O_{12}S_8$: C 71.18, H 6.67; found: C 70.81, H 6.64.

General procedure for the preparation of the [2]rotaxanes: A solution of the dumbbell-shaped compounds **7**, **8**, **9**, **10**, **11**, or **12** (0.035 mmol), the dicationic salt **18**·2PF$_6$ (74 mg, 0.105 mmol) and the dibromide **17** (28 mg, 0.105 mmol) in anhydrous DMF (10 mL) was stirred at room temperature for 10 d (after approximately 2 d the color changed to dark purple (for DNP) or dark green (for TTF) and a white precipitate formed). After removal of the solvent, the residue was subjected to column chromatography (SiO_2) and unreacted dumbbell-shaped compounds was eluted with Me_2CO, whereupon the eluent was changed to Me_2CO/NH_4PF_6 (1.0 g NH_4PF_6 in 100 mL Me_2CO) and the colored band containing the [2]rotaxanes was collected. Most of the solvent was removed under vacuum. After adding H_2O (50 mL) to the residue, the precipitate was collected by filtration, washed with Et_2O (30 mL), and dried in vacuo to afford the [2]rotaxanes.

Compound 1·4PF$_6$: Yield: 54%; m.p. 256–258°C; UV/Vis (MeCN): $\lambda_{max} = 514$ nm; ^{1}H NMR (CD_3CN, 500 MHz): $\delta = 1.06$–1.15 (m, 6H), 1.20, 1.26 (2 × s, 36H), 2.18–2.23 (m, 1H), 2.24–2.31 (m, 1H), 2.47–2.63 (m, 4H), 3.54–4.41 (m, 32H), 5.53–5.81 (m, 8H), 5.81–5.89 (m, 1H), 6.03–6.10 (m, 1H), 6.11–6.18 (m, 1H), 6.31–6.38 (m, 1H), 6.57–6.74 (m, 2H), 6.77–7.33 (m, 42H), 7.78–8.04 (m, 10H), 8.29–8.45 (m, 4H), 8.63–8.81 (m, 2H), 8.86–9.01 ppm (m, 2H); MS (FAB): *m/z* (%): 2526 (15) $[M-PF_6]^+$, 2381 (30) $[M-2PF_6]^+$, 2236 (10) $[M-3PF_6]^+$; elemental analysis calcd (%) for $C_{142}H_{154}N_4O_{11}P_4F_{24}$: C 63.81, H 5.81, N 2.10; found: C 62.90, H 5.98, N 2.00.

Compound 2·4PF$_6$: Yield: 51%; m.p. 106–108°C (decomp); UV/Vis (MeCN): $\lambda_{max} = 846$ nm; ^{1}H NMR (CD_3CN, 500 MHz): $\delta = 1.17$ (t, $J = 7.6$ Hz, 6H), 1.26 (s, 36H), 2.57 (m, 4H), 3.20–4.28 (m, 40H), 5.47–5.83 (m, 8H), 6.01–6.36 (m, 4H), 6.49–6.64 (m, 2H), 6.66–6.82 (m, 2H), 6.96–7.17 (m, 20H), 7.19–7.33 (m, 8H), 7.51–7.95 (m, 16H), 8.75–9.15 ppm (m, 8H); MS (FAB): *m/z* (%): 2734 (5) $[M-PF_6]^+$, 2589 (4) $[M-2PF_6]^+$; elemental analysis calcd (%) for $C_{138}H_{154}N_4O_{11}P_4S_8F_{24}$: C 57.53, H 5.39, N 1.94; found: C 59.85, H 5.23, N 1.99.

Compound 3·4PF$_6$: Yield: 25%; m.p. 251–253°C; UV/Vis (MeCN): $\lambda_{max} = 516$ nm; ^{1}H NMR (CD_3CN, 500 MHz): $\delta = 1.11$–1.18 (m, 6H), 1.19–1.28 (br, 36H), 2.31–2.39 (m, 2H), 2.51–2.60 (m, 4H), 3.80–4.00 (m, 8H), 4.04–4.12 (m, 2H), 4.13–4.34 (m, 16H), 4.36–4.48 (m, 4H), 4.71–4.79 (m, 2H), 5.55–5.74 (m, 8H), 5.86–5.98 (m, 2H), 6.17–6.28 (m, 2H), 6.71–6.85 (m, 6H), 6.86–6.93 (m, 2H), 6.94–7.00 (m, 2H), 7.01–7.14 (m, 24H), 7.15–7.35 (m, 14H), 7.62–7.72 (m, 2H), 7.80–8.10 (m, 12H), 8.46–8.71 (m, 4H), 8.71–8.99 ppm (m, 2H); MS(FAB): *m/z* (%): 2767 (12) $[M-PF_6]^+$, 2621 (8) $[M-2PF_6]^+$, 2476 (7) $[M-3PF_6]^+$; elemental analysis calcd (%) for $C_{156}H_{162}N_4O_{15}P_4F_{24}$: C 64.32, H 5.61, N 1.92; found: C 62.71, H 5.46, N 1.85.

Compound 4·4PF$_6$: Yield: 11%; m.p. 221–221°C; ^{1}H NMR (CD_3CN, 500 MHz): $\delta = 1.17$ (2×t, $J = 7.5$ Hz, 6H), 1.23–1.27 (m, 36H), 2.57 (q, $J = 7.5$ Hz, 4H), 3.52–4.58 (m, 20H), 5.49–5.68 (m, 8H), 6.00, 6.04, 6.20, 6.21 (4×s, 2H), 6.52, 6.53, 6.56, 6.58 (4×s, 2H), 7.09–7.16 (m, 20H), 7.30 (d, $J = 8.4$ Hz, 8H), 8.09 (d, $J = 8.5$ Hz, 4H), 6.76–9.00 ppm (m, 52H); MS (FAB): *m/z* (%): 2974 (10) $[M-PF_6]^+$, 2831 (9) $[M-2PF_6]^+$.

Compound 5·4PF$_6$: Yield: 25%; m.p. 252–254°C; UV/Vis (MeCN): $\lambda_{max} = 519$ nm; ^{1}H NMR (CD_3COCD_3, 500 MHz): $\delta = 1.13$–1.21 (m, 6H), 1.21–1.34 (s, 36H), 2.53–2.61 (m, 4H), 2.72–2.80 (m, 2H), 3.87–4.68 (m, 32H), 5.93–6.15 (m, 8H), 6.20–6.38 (m, 2H), 6.39–6.60 (m, 2H), 6.77–7.16 (m, 32H), 7.19–7.37 (m, 10H), 7.45–7.66 (m, 6H), 7.69–7.96 (m, 10H), 8.15–8.52 (m, 8H), 9.10–9.51 ppm (m, 8H); MS (FAB): *m/z* (%): 2771 (10) $[M-PF_6]^+$; elemental analysis calcd (%) for $C_{160}H_{165}N_4O_{12}P_4F_{24}$: C 65.90, H 5.70, N 1.92; found: C 64.16, H 5.76, N 1.66.

Compound 6·4PF$_6$: Yield: 51%; m.p. 228°C (decomp); UV/Vis (MeCN): $\lambda_{max} = 846$ nm; ^{1}H NMR (CD_3COCD_3, 500 MHz): $\delta = 1.11$–1.19 (m, 6H), 1.20–1.30 (m, 36H), 2.51–2.61 (m, 4H), 3.51–4.36 (m, 40H), 5.82–5.95 (m, 4H), 5.96–6.08 (m, 4H), 6.20, 6.25, 6.34, 6.38 (4 ? s, 4H), 6.48 (m, 1H), 6.61–6.84 (m, 7H), 6.95–7.11 (m, 20H), 7.19–7.30 (m, 8H), 7.35–7.62 (m, 8H), 7.82–7.99 (m, 8H), 8.10–8.38 (m, 8H), 9.33–9.50 ppm (m, 8H); MS (ESI): *m/z* (%): 1418 $[M-2PF_6]^{2+}$, 897 $[M-3PF_6]^{3+}$; elemental analysis calcd (%) for $C_{156}H_{166}N_4O_{12}S_8P_4F_{24}$: C 59.95, H 5.35, N 1.79; found: C 59.99, H 5.37, N 1.75.

Acknowledgment

This research was supported by the Defense Advanced Research Projects Agency (DARPA). Part of this work is based upon research supported by the National Science Foundation under equipment grant CHE-9974928.

[1] a) J. F. Stoddart, *Chem. Aust.* **1992**, *59*, 576–577, 581; b) M. Gómez-López, J. A. Preece, J. F. Stoddart, *Nanotechnology* **1996**, *7*, 183–192; c) V. Balzani, M. Gómez-López, J. F. Stoddart, *Acc. Chem. Res.* **1998**, *31*, 405–414; d) V. Balzani, A. Credi, F. M. Raymo, J. F. Stoddart, *Angew. Chem.* **2000**, *112*, 3484–3530; *Angew. Chem. Int. Ed.* **2000**, *39*, 3348–3391; e) H.-R. Tseng, J. F. Stoddart, *Modern Arene Chemistry* (Ed.: D. Astruc), Wiley-VCH, **2002**, pp. 574–599.

[2] a) A. Harada, *Acc. Chem. Res.* **2001**, *34*, 456–464; b) C. A. Schalley, K. Beizai, F. Vögtle, *Acc. Chem. Res.* **2001**, *34*, 465–476; c) J.-P. Collin, C. Dietrich-Buchecker, P. Gaviña, M. C. Jimenez-Molero, J.-P. Sauvage, *Acc. Chem. Res.* **2001**, *34*, 477–487; d) R. Ballardini, V. Balzani, A. Credi, M. T. Gandolfi, M. Venturi, *Struct. Bonding* **2001**, *99*, 55–78; e) C. A. Stanier, S. J. Alderman, T. D. W. Claridge, H. L. Anderson, *Angew. Chem.* **2002**, *114*, 1847–1850; *Angew. Chem. Int. Ed.* **2002**, *41*, 1769–1772; f) V. Balzani, A. Credi, M. Venturi, *Chem. Eur. J.* **2002**, *8*, 5524–5532; g) V. Balzani, A. Credi, M. Venturi, *Molecular Devices and Machines—A Journey into the Nano World*, Wiley-VCH, Weinheim, **2003**.

[3] a) A. Aviram, M. A. Ratner, *Chem. Phys. Lett.* **1974**, *29*, 277–283; b) R. M. Metzger, J. W. Baldwin, W. J. Shumate, I. R. Peterson, P. Mani, C. J. Mankey, T. Morris, G. Szulczewski, S. Bosi, M. Prato, A. Comito, Y. Rubin, *J. Phys. Chem. B* **2003**, *107*, 1021–1027; c) J. Park, A. N. Pasupathy, J. I. Goldsmith, C. Chang, Y. Yaish, J. R. Petta, M. Rinkoski, J. P. Sethna, H. D. Abruña, P. L. McEuen, D. C. Ralph, *Nature* **2002**, *417*, 722–725; d) W. Liang, M. P. Shores, M. Brockrath, J. R. Long, H. Park, *Nature* **2002**, *417*, 725–729.

[4] a) C. P. Collier, G. Mattersteig, E. W. Wong, Y. Luo, K. Beverly, J. Sampaio, F. M. Raymo, J. F. Stoddart, J. R. Heath, *Science* **2000**, *289*, 1172–1175; b) A. R. Pease, J. O. Jeppesen, J. F. Stoddart, Y. Luo, C. P. Collier, J. R. Heath, *Acc. Chem. Res.* **2001**, *34*, 433–444; c) Y. Luo, C. P. Collier, J. O. Jeppesen, K. A. Nielsen, E. DeIonno, G. Ho, J. Perkins, H.-R. Tseng, T. Yamamoto, J. F. Stoddart, J. R. Heath, *ChemPhysChem* **2002**, *3*, 519–525; d) M. R. Diehl, D. W. Steuerman, H.-R. Tseng, S. A. Vignon, A. Star, P. C. Celestre, J. F. Stoddart J. R. Heath, *ChemPhysChem* **2003**, *4*, 1335–1339.

[5] Both semiconductors (Heath group at Caltech) and metals (Williams group at Hewlett Packard) have been used as the bottom electrode for molecular electronic devices incorporating bistable [2]catenanes and [2]rotaxanes. Recently, it has been established that the devices incorporating metals (See: Y. Chen, D. A. A. Ohlberg, X. Li, D. R. Stewart, R. S. Williams, J. O. Jeppesen, K. A. Nielsen, J. F. Stoddart, D. L. Olyniek, E. Anderson, *Appl. Phys. Lett.* **2003**, *82*, 1610–1612; Y. Chen, G.-Y. Jung, D. A. A. Ohlberg, X. Li, D. R. Stewart, J. O. Jeppesen, K. A. Nielsen, J. F. Stoddart, R. S. Williams, *Nanotechnology* **2003**, *14*, 462–468; D. R. Stewart, D. A A. Ohlberg, P. A. Beck, Y. Chen, R. S. Williams, J. O. Jeppesen, K. A. Nielsen, J. F. Stoddart, *Nano Lett.* **2004**, *4*, 133–136) as the bottom electrode

do not switch as a result of a molecular-based process. Rather, the observed bistability is probably a result of reversible filament growth between the two electrodes. This result does *not* pertain, however, to devices incorporating semiconductors (polysilicon, for example) as the bottom electrode. To date, all of the available experimental evidence suggests that the devices incorporating semiconducting bottom electrodes switch as a consequence of a molecularly based electromechanical mechanism at low bias voltages (± 2 V).

[6] V. Balzani, A. Credi, F. M. Raymo, J. F. Stoddart, *Angew. Chem.* **2000**, *112*, 3484–3530; *Angew. Chem. Int. Ed.* **2000**, *39*, 3348–3391.

[7] a) M. Asakawa, P. R. Ashton, V. Balzani, A. Credi, C. Hamers, G. Mattersteig, M. Montalti, A. N. Shipway, N. Spencer, J. F. Stoddart, M. S. Tolley, M. Venturi, A. J. P. White, D. J. Williams, *Angew. Chem.* **1998**, *110*, 357–361; *Angew. Chem. Int. Ed.* **1998**, *37*, 333–337; b) V. Balzani, A. Credi, G. Mattersteig, O. A. Matthews, F. M. Raymo, J. F. Stoddart, M. Venturi, A. J. P. White, D. J. Williams, *J. Org. Chem.* **2000**, *65*, 1924–1936.

[8] a) J. O. Jeppesen, K. A. Nielsen, J. Perkins, S. A. Vignon, A. Di Fabio, R. Ballardini, M. T. Gandolfi, M. Venturi, V. Balzani, J. Becher, J. F. Stoddart, *Chem. Eur. J.* **2003**, *9*, 2982–3007; b) T. Yamamoto, H.-R. Tseng, J. F. Stoddart, V. Balzani, A. Credi, F. Marchioni, M. Venturi, *Collect. Czech. Chem. Commun.* **2003**, *68*, 1488–1514; c) H.-R. Tseng, S. A. Vignon, P. C. Celestre, J. Perkins, J. O. Jeppesen, A. Di Fabio, R. Ballardini, M. T. Gandolfi, M. Venturi, V. Balzani, J. F. Stoddart, *Chem. Eur. J.* **2004**, *10*, 155–172.

[9] H.-R. Tseng, D. Wu, N. X. Fang, X. Zhang, J. F. Stoddart, *ChemPhysChem* **2004**, *5*, 111–116.

[10] a) C. L. Brown, U. Jonas, J. A. Preece, H. Ringsdorf, M. Seitz, J. F. Stoddart, *Langmuir* **2000**, *16*, 1924–1930; b) M. Asakawa, M. Higuchi, G. Mattersteig, T. Nakamura, A. R. Pease, F. M. Raymo, T. Shimizu, J. F. Stoddart, *Adv. Mater.* **2000**, *12*, 1099–1102; c) C. P. Collier, J. O. Jeppesen, Y. Luo, J. Perkins, E. W. Wong, J. R. Heath, J. F. Stoddart, *J. Am. Chem. Soc.* **2001**, *123*, 12632–12641.

[11] For a discussion of first-principles computational methods which indicate that, when the $CBPQT^{4+}$ ring surrounds the DNP ring system, the switch is ON, whereas, when it surrounds the TTF unit, the switch is OFF, see: A. H. Flood, R. J. A. Ramirez, W. Deng, R. P. Muller, W. A. Goddard III, J. F. Stoddart, *Aust. J. Chem.*, in press results. The difference in conductivity between these two states is considered to be due to a change in the degree of delocalization of the molecular orbitals when the ring is located around the TTF unit, as opposed to when it encircles the DNP ring system. In the case where the $CBPQT^{4+}$ ring is located around the TTF unit, the HOMO is localized on the TTF unit, while the LUMO is localized on the DNP ring system. In the metastable state, where the ring encircles the DNP ring system, the HOMO and LUMO are both delocalized across both recognition sites. See also a report on "Computational Nanotechnology" by E. K. Wilson, *Chem. Eng. News* **2003**, April 28, 27–29.

[12] The electromechanical switching mechanism has been investigated for similar molecules in a half-device (ref. [9]) and in a polymer electrolyte thin film (unpublished results). The barrier for relaxation of the metastable state to the ground state was determined by performing cyclic voltammetry experiments at a series of temperatures in these devices, and found to be ~18 and ~21 kcal mol^{-1}, respectively. This result can be compared to the barrier for shuttling in the degenerate DNP-containing rotaxanes reported here, where the barrier is ~15 kcal mol^{-1}.

[13] H.-R. Tseng, S. A. Vignon, J. F. Stoddart, *Angew. Chem.* **2003**, *115*, 1529–1533; *Angew. Chem. Int. Ed.* **2003**, *42*, 1491–1495.

[14] a) P. R. Ashton, T. T. Goodnow, A. E. Kaifer, M. V. Reddington, A. M. Z. Slawin, N. Spencer, J. F. Stoddart, C. Vicent, D. J. Williams, *Angew. Chem.* **1989**, *101*, 1404–1408; *Angew. Chem. Int. Ed. Engl.* **1989**, *28*, 1396–1399; b) P.-L. Anelli, P. R. Ashton, R. Ballardini, V. Balzani, M. Delgado, M. T. Gandolfi, T. T. Goodnow, A. E. Kaifer, D. Philp, M. Pietraszkiewicz, L. Prodi, M. V. Reddington, A. M. Z. Slawin, N. Spencer, J. F. Stoddart, C. Vicent, D. J. Williams, *J. Am. Chem. Soc.* **1992**, *114*, 193–218.

[15] a) P.-L. Anelli, N. Spencer, J. F. Stoddart, *J. Am. Chem. Soc.* **1991**, *113*, 5131–5133; b) P.-L. Anelli, M. Asakawa, P. R. Ashton, R. A. Bissell, G. Clavier, R. Górski, A. E. Kaifer, S. J. Langford, G. Mattersteig, S. Menzer, D. Philp, A. M. Z. Slawin, N. Spencer, J. F. Stoddart, M. S. Tolley, D. J. Williams, *Chem. Eur. J.* **1997**, *3*, 1113–1135; c) D. A. Leigh, A. Troisi, F. Zerbetto, *Angew. Chem.* **2000**, *112*, 358–361; *Angew. Chem. Int. Ed.* **2000**, *39*, 350–353; d) J. Cao, M. C. T. Fyfe, J. F. Stoddart, G. R. L. Cousins, P. T. Glink, *J. Org. Chem.* **2000**, *65*, 1937–1946; e) A. M. Elizarov, T. Chang, S.-H. Chiu, J. F. Stoddart, *Org. Lett.* **2002**, *4*, 3565–3568.

[16] a) S. Anderson, H. L. Anderson, J. K. M. Sanders, *Acc. Chem. Res.* **1993**, *26*, 469–475; b) J. P. Schneider, J. W. Kelly, *Chem. Rev.* **1995**, *95*, 2169–2187; c) F. M. Raymo, J. F. Stoddart, *Pure Appl. Chem.* **1996**, *68*, 313–322; d) *Templated Organic Synthesis* (Eds.: F. Diederich, P. J. Stang), Wiley-VCH, Weinheim, **1999**; e) J. F. Stoddart, H.-R. Tseng, *Proc. Natl. Acad. Sci. USA* **2002**, *99*, 4797–4800.

[17] The tosylate **14** was synthesized by reacting 4-[4-ethylphenyl-bis(4-*tert*-butylphenyl)methyl]phenol with the ditosylate of 1,5-bis[2(hydroxyethoxy)ethoxy]-naphthalene in MeCN in the presence of LiBr and K_2CO_3.

[18] J. O. Jeppesen, J. Perkins, J. Becher, J. F. Stoddart, *Angew. Chem.* **2001**, *113*, 1256–1261; *Angew. Chem. Int. Ed.* **2001**, *40*, 1216–1221.

[19] a) B. Odell, M. V. Reddington, A. M. Z. Slawin, N. Spencer, J. F. Stoddart, D. J. Williams, *Angew. Chem.* **1988**, *100*, 1605–1608; *Angew. Chem. Int. Ed.* **1998**, *27*, 1547–1550; b) P. R. Ashton, B. Odell, M. V. Reddington, A. M. Z. Slawin, J. F. Stoddart, D. J. Williams, *Angew. Chem.* **1988**, *100*, 1608–1611; *Angew. Chem. Int. Ed.* **1998**, *27*, 1550–1553; c) M. Asakawa, W. Dehaen, G. L'abbé, S. Menzer, J. Nouwen, F. M. Raymo, J. F. Stoddart, D. J. Williams, *J. Org. Chem.* **1996**, *61*, 9591–9595; d) G. Doddi, G. Ercolani, S. Franconeri, P. Mencarelli, *J. Org. Chem.* **2001**, *66*, 4950–4953; e) G. Ercolani, P. Mencarelli, *J. Org. Chem.* **2003**, *68*, 6472–6473 f) C. D'Acerno, G. Doddi, G. Ercolani, S. Franconeri, P. Mencarelli, A. Piermattei, *J. Org. Chem.* **2004**, *69*, 1393–1396.

[20] Y.-K. Han, A. Reiser, *Macromolecules* **1998**, *31*, 8789–8793.

[21] a) M. Feigel, H. Kessler, D. Leibfritz, *J. Am. Chem. Soc.* **1979**, *101*, 1943–1950; b) B. E. Mann, *J. Magn. Reson.* **1977**, *25*, 91–94.

[22] Partial NMR spectra were simulated and compared to the recorded experimental spectra by using SpinWorks 2.1, K. Marat, Department of Chemistry, University of Manitoba (Canada).

[23] The rate of shuttling in the TTF-containing rotaxanes was estimated by determining an average value ($\Delta\nu_{ex}\sim 7\ s^{-1}$) of the peak separations for the many signals arising from *tert*-butyl groups in their hydrophobic stoppers at low temperatures and coming up with an estimate (320 K) for the coalescence temperature, T_c. This information was then inserted into the equation, $k_c=(\pi\Delta\nu_{ex})/2^{1/2}$, to determine the rate of exchange, k_c, which was estimated to be $\sim 16\ s^{-1}$ at the T_c of ~320 K. By using the Eyring equation, $\Delta G_c^{\ddagger}=RT_c\ln(k_c h/k_b T_c)$, in which R is the gas constant, h is Planck's constant, and k_b is Boltzmann's constant, this rate constant (k_c) corresponds to a $\Delta G_c^{\ddagger}$ of ~17 kcal mol^{-1} at T_c. The rate constants at the appropriate coalescence temperatures for all three [2]rotaxanes, containing two TTF recognition sites, gave $\Delta G_c^{\ddagger}$ values ranging from 17–18 kcal mol^{-1}. These results should be compared with those reported previously for a TTF-based [2]pseudorotaxane for which the "shuttling" mechanism is probably bimolecular, see: M. R. Bryce, G. Cooke, W. Devonport, F. M. A. Duclairoir, V. M. Rotello, *Tetrahedron Lett.* **2001**, *42*, 4223–4226.

[24] V. Balzani, A. Credi, G. Mattersteig, O. A. Matthews, F. M. Raymo, J. F. Stoddart, M. Venturi, A. J. P. White, D. J. Williams, *J. Org. Chem.* **2000**, *65*, 1924–1936.

[25] R. Castro, K. R. Nixon, J. D. Evenseck, A. E. Kaifer, *J. Org. Chem.* **1996**, *61*, 7298–7303.

[26] P. R. Ashton, R. Ballardini, V. Balzani, M. Belohradsky, M. T. Gandolfi, D. Philp, L. Prodi, F. M. Raymo, M. V. Reddington, N. Spencer, J. F. Stoddart, M. Venturi, D. J. Williams, *J. Am. Chem. Soc.* **1996**, *118*, 4931–4951.

[27] D. B. Amabilino, C. O. Dietrich-Buchecker, A. Livoreil, L. Pérez-García, J.-P. Sauvage, J. F. Stoddart, *J. Am. Chem. Soc.* **1996**, *118*, 3905–3913.

Received: November 17, 2003 [F5725]

Published online: March 23, 2004